Hindawi
Journal of Nanomaterials
Volume 2018, Article ID 9235263, 10 pages
https://doi.org/10.1155/2018/9235263

Research Article

Synthesis of Encapsulated Zn(8-hydroxyquinoline)$_2$(H_2O)$_2$ in the Pore of BioMOF1 for Sensing Dissolved Oxygen in Water

Phakinee Srilaoong,[1] Jiraporn Buasakun,[1] Kittipong Chainok,[2] Boontana Wannalerse,[1] Ramida Rattanakam,[1] and Tanwawan Duangthongyou[1]

[1]*Department of Chemistry, Faculty of Science, Kasetsart University, Bangkok 10900, Thailand*
[2]*Materials Innovation and Technology, Department of Physics, Faculty of Science and Technology, Thammasat University, Pathum Thani 12120, Thailand*

Correspondence should be addressed to Tanwawan Duangthongyou; fscitwd@ku.ac.th

Received 6 November 2017; Revised 10 January 2018; Accepted 28 January 2018; Published 26 February 2018

Academic Editor: Sheng-Joue Young

The Zn(8-hydroxyquinoline)$_2$(H_2O)$_2$, $ZnQ_2{\cdot}2H_2O$, encapsulated in the porous BioMOF1 (ZnQ_2@BioMOF1) host was synthesized by solid-solid and solid-solution reaction between Zn^{2+}@BioMOF1 and 8-hydroxyquinoline. To prepare Zn^{2+}@BioMOF1, dimethylammonium (DMA^+), guests in the pores of BioMOF1 were replaced by Zn^{2+} ions via ion exchange process. The synthesized compound was characterized by XRD and TGA to confirm stability of BioMOF1 host. The $ZnQ_2{\cdot}2H_2O$ forming by metal-cation-directed de novo coassembly approach was confirmed by UV, IR, Fluorescence, BET, and confocal microscopy. Scanning electron microscopy images show slight change in morphology of BioMOF1 after introducing $ZnQ_2{\cdot}2H_2O$ by solid-solution reaction into its pores. Thin films of the produced materials were used to sense dissolved oxygen in water by using fluorescence technique.

1. Introduction

Metal-organic frameworks (MOFs) are a new class of synthetic porous materials built up with metal ions/clusters and organic linkers. Depending on the selected metal ions, molecular linkers, and the synthetic conditions, MOFs develop a variety of molecular topologies, usually with large internal space, which contributes to their prominent features including high specific surface area and pore volume. These materials have attracted attentions from academic and industry around the globe over this period. They have shown a wide range of potential applications such as gas storage [1], catalysis [2], drug delivery [3], and optical and chemical sensing [4]. Recently, new MOF materials with tunable luminescent properties have been designed [5, 6]. Encapsulation of guest molecules in space of MOFs has been considered an effective concept for fabricating novel functional materials. By using MOFs as a host, functional guest species, for example, metal ions, organometallic complexes, quantum dots, nanoparticles, and fluorescent dyes, are stabilized and confined within the pores, leading to specific behaviors that improve and broaden properties of MOFs towards advanced gas storage materials, optical devices, heterogeneous catalysts, and sensors [7–13]. Interestingly, the fluorescence behavior of MOFs can even be further tuned by encapsulating guest species such as cations, anions, and solvent molecules [14, 15].

There are several methods to include functionalized guest molecules into the pores of MOFs such as impregnation [16], chemical vapor deposition [17], cation exchange [18], and coassembly [19, 20]. However, the ability to incorporate the guests is limited by the size of the pores as the pores are likely to be inaccessible to guests with larger size compared to pore size of MOF hosts. To solve that problem, a new alternative approach has been developed, namely, "metal-cation-directed de novo assembly" or "ship-in-a-bottle" [21–23]. This approach is based on the formation of functional guest molecules from its fragments by introduction of metal ions to MOF prior to the assembly of component fragments under the direction of metal ions.

In this research BioMOF1 was selected to be a host because it has high specific surface area (~1700 m^2/g) and

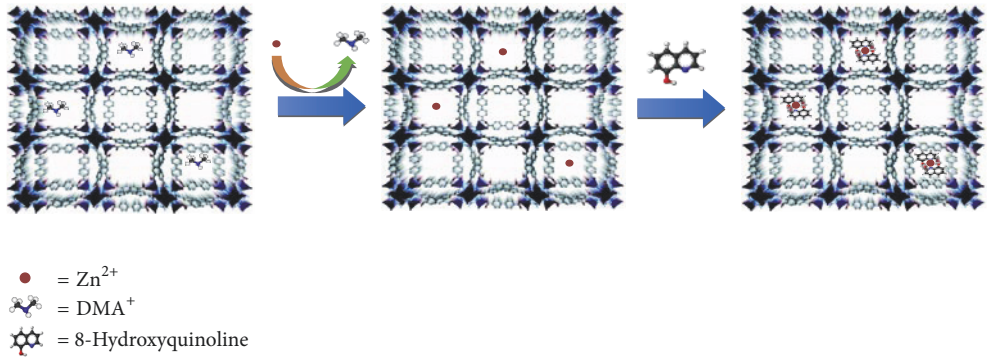

Scheme 1: Procedure for encapsulating guest molecule into metal-organic framework.

pore aperture of 5.2 Å [24]. In addition, the BioMOF1 is an anionic complex encapsulated with dimethylammonium cation (the product of DMF decomposition) in the cavity.

8-Hydroxyquinoline metal chelate, Zn-bis(8-hydroxyquinoline), is under intensive research due to its excellent fluorescence properties. Quinoline derivatives have gained a lot of attention due to their photoluminescence and electroluminescence properties. These properties are very sensitive to the change of electron vibration shift in their structures [25]. They are useful materials for electroluminescent application especially for light emitting diodes (LED). Recent reports have shown that Zn(8-hydroxyquinoline)$_2$(H_2O)$_2$, or (ZnQ_2·$2H_2O$), can be synthesized simply by a room temperature solid-state reaction [26]. As it is well known that oxygen molecules are able to quench fluorescence, therefore the fluorescence properties of ZnQ_2·$2H_2O$ will be quenched when oxygen molecules are present. This complex can be an alternative dye for oxygen sensor.

Dissolved oxygen in water plays an important role in biological, clinical, environmental, and industrial applications. Several oxygen detection methods have been reported, mainly based on electrochemical, optical, and chemical processes. Electrochemical method is the most popular due to the conventional procedure in measuring oxygen concentration. However, this method tends to suffer from the instability of electrode surface. Optical oxygen sensor offers inexpensive highly sensitive measurement and fast response. Most optical oxygen sensors are based on luminescence quenching of sensitive dyes, which are commonly transition metal complexes. Ru(II) polypyridine complexes immobilized in polymer films have been employed more frequently [27–31] during the early stage. Later, polypyridine complexes of Osmium(II) [32], Rhenium(I) [33], Platinum(II) [34], and Irridium(II) [35] have also been investigated. These transition metal complexes possess high emission metal-to-ligand charge transfer (MLCT), therefore representing good oxygen sensitive dyes.

Moreover to improve the quantum yield and lifetime of the organic dyes, oxygen permeability of polymer matrixes is more concentrated on such as using fluoropolymer [35, 36], organically modified silicates (ORMOSIL) [37], silicone matrix [38], and so on. Optical oxygen sensors have been further developed in many procedures. Material based on a Ru(II) polypyridine complex encapsulated in zeolite Y was reported compared with one adsorbed on the surface. It was found that oxygen quenching was higher in encapsulating material [39]. Recently, Zn(8-hydroxyquinoline)$_2$ intercalated in calcium bentonite coated on a polystyrene sheet was used to measure dissolved oxygen [40].

Herein, we report the facile synthesis and characterization of a novel oxygen sensing material comprising Zn(8-hydroxyquinoline)$_2$(H_2O)$_2$, or (ZnQ_2·$2H_2O$), encapsulated in the pores of BioMOF1 (Scheme 1). The incorporation of ZnQ_2·$2H_2O$ into the MOF structure was done via metal-cation-directed de novo assembly through solid-state reaction and solid-solution reaction. Dissolved oxygen sensing property of this material was studied by fluorescence-based measurement.

2. Materials and Methods

2.1. Materials and Measurements. All reagents were purchased from commercial sources and used as received. Infrared (IR) spectra were measured in KBr pellets on a Bruker Model Equinox 55 spectrophotometer in the region 400–4000 cm^{-1}. Thermogravimetric analyses (TGA) were studied by a Perkin Elmer TGA7 with a heating rate of 10°C per min under N_2. UV-VIS diffuse reflectance spectra were recorded between 200 and 1000 nm by using UV-VIS Spectrophotometer Shimadzu UV-2600. Fluorescence emission spectra were measured on a Perkin Klmer model LS55 Luminescence spectrometer. Elemental analyses (C, H, and N) were studied by a LECO CHNS-932. Powder X-ray diffraction patterns (PXRD) were collected on a D8 Advance Bruker X-ray diffractometer using Cu-Kα radiation (λ = 1.54060 Å). Scanning electron microscopy (SEM) was carried out on a Quanta 450 FEI with Tungsten filament electron source operated at 25 kV. Fluorescence quantum yield and fluorescence lifetime were measured in solid-state with Spectrofluorometer HORIBA Fluoromax model. The fluorescence images were obtained with a Nikon C2-si laser scanning confocal microscope.

2.2. Synthesis of Zn^{2+}@BioMOF1. BioMOF1 was synthesized according to the previous work [24]. Typically, Adenine (0.125 mmol), 4,4′-biphenyl dicarboxylic acid (BPDC)

(0.25 mmol), zinc acetate dihydrate (0.375 mmol), nitric acid (1 mmol), DMF (13.5 mL), and water (1 mL) were added to a Teflon-lined autoclave at 130°C for 24 h. Rod-shaped colorless crystals were produced. The crystals were collected, washed with DMF (3 mL × 3), and dried. The prepared BioMOF1 was soaked in DMF solution of $Zn(NO_3)_2$ and heated at 65°C for 24 h. Then the resulting product was washed with DMF three times and dried in the oven. The obtained solid was called Zn^{2+}@BioMOF1.

2.3. Synthesis of ZnQ_2@BioMOF1

2.3.1. Solid-Solution Reaction. Zn^{2+}@BioMOF1 powder was immersed in the DMF solution of 8-hydroxyquinoline for 24 h. The supernatant solution was decanted and fresh 8-hydroxyquinoline in DMF solution was refilled. This procedure was repeated a time a day for 3 days.

2.3.2. Solid-Solid Reaction. A 1 : 2 ratio of Zn^{2+}@BioMOF1 and 8-hydroxyquinoline was mixed and ground in a mortar for 20 min. The color of the mixture changed from white to yellow within a few seconds. Then the mixture was washed with ethanol to remove the unreacted starting materials. The product was dried at 363 K and used for further characterization. $ZnQ_2{\cdot}2H_2O$ was also prepared as a reference via solid-solid reaction according to the previously reported procedure [26].

2.4. Preparation of ZnQ_2@BioMOF1 Film. The sensor film was prepared using the method adopted from the literature [40]. Briefly, 1 g of polystyrene pellets was dissolved in 5 ml toluene and the obtained solution was mixed with ZnQ_2@BioMOF1 (2 : 1 by weight, respectively); then the mixture was coated manually as a film on cleaned polystyrene sheets.

2.5. Preparation of Dissolved Oxygen Water Samples. To obtain 0%, 10%, 20%, 30%, 50%, 60%, 70%, 80%, 90%, and 100% dissolved oxygen in water (DO water), different ratios of nitrogen and oxygen gas mixtures were flown into deionized (DI) water. For example, 50 ml/min of oxygen gas was mixed with 450 ml/min of nitrogen, the flow rate of which was controlled by mass flow controllers, in order to produce the gas mixture containing 10% of O_2. This gas mixture was then allowed to flow into the chamber containing deionized for 30 min. The resultant water sample was labelled as 10% dissolved oxygen in water.

2.6. Fluorescence Measurement. The sensor films were placed into diagonally fluorescent cuvette. The efficacy of sensor films was measured by adding dissolved oxygen water (DO water) at various concentrations. The changes in fluorescent response were recorded by excitation at wavelength of 380 nm.

3. Results and Discussion

XRD patterns of the prepared BioMOF1 host and its guest-encapsulated versions are shown in Figure 1. The pattern of

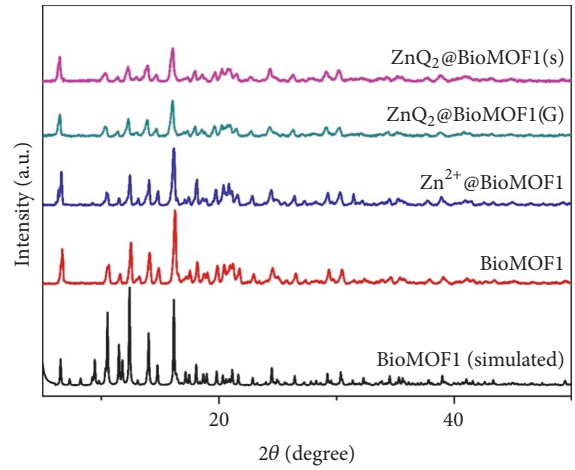

Figure 1: Comparison of the experimental powder XRD patterns of the synthesized materials.

the prepared BioMOF1 is in agreement with the simulated pattern, indicating that BioMOF1 framework was successfully synthesized. After the prepared BioMOF1 was immersed in DMF solution of Zn(II) ions, dimethylammonium cation (DMA^+) guests in the pores of BioMOF1 were substituted by Zn(II) ions from the solution through cation ion exchange process, allowing the formation of Zn^{2+}@BioMOF1. The XRD pattern of Zn^{2+}@BioMOF1 was not changed after Zn^{2+} incorporation and showed the same reflections as the parent BioMOF1, which illustrates that the framework of BioMOF1 host was stable upon cation ion exchange during soaking step.

In order to form ZnQ_2-encapsulated BioMOF1, 8-hydroxyquinoline (Q) molecules were incorporated into Zn^{2+}@BioMOF1 using two different approaches including solid-solution and solid-solid reactions, later yielding ZnQ_2@BioMOF1(S) and ZnQ_2@BioMOF1(G), respectively. For both reactions, the white color of Zn^{2+}@BioMOF1 turned to yellow after Zn^{2+}@BioMOF1 reacted with 8-hydroxyquinoline, confirming the formation of Zn-8-hydroquinoline complex, $ZnQ_2{\cdot}2H_2O$, and corresponding ZnQ_2@BioMOF1. The XRD patterns of ZnQ_2@BioMOF1(S) and ZnQ_2@BioMOF1(G) are in good agreement with Zn^{2+}@BioMOF1, which suggests that the encapsulation of ZnQ_2 did not disrupt the crystal structure of BioMOF1 and the formation of ZnQ_2@BioMOF1 can be achieved either by using solid-solution or solid-solid reaction. No diffraction peaks from $ZnQ_2{\cdot}2H_2O$ were detected; this is likely because of the low content and the small size of $ZnQ_2{\cdot}2H_2O$ formed inside the pores of BiOMOF1 framework.

Figure 2 shows thermal gravimetric analysis of the parent BioMOF1 and its guest-encapsulated products. The percentages of elements found in the prepared BioMOF1, $(Zn_8(ad)_4(BPDC)_6O{\cdot}2Me_2NH_2{\cdot}8DMF{\cdot}10H_2O)$, are C, 46.53; H, 4.83; N, 12.80 (Anal. Calc.: C, 46.76; H, 5.07; N, 12.40). For the parent BioMOF1, the first weight loss up to 170°C, approximately 23.85%, was due to the loss of 10 water and 8 DMF molecules as calculated from elemental analysis results (calc. 22.5%). The second weight loss of about 2.13% observed

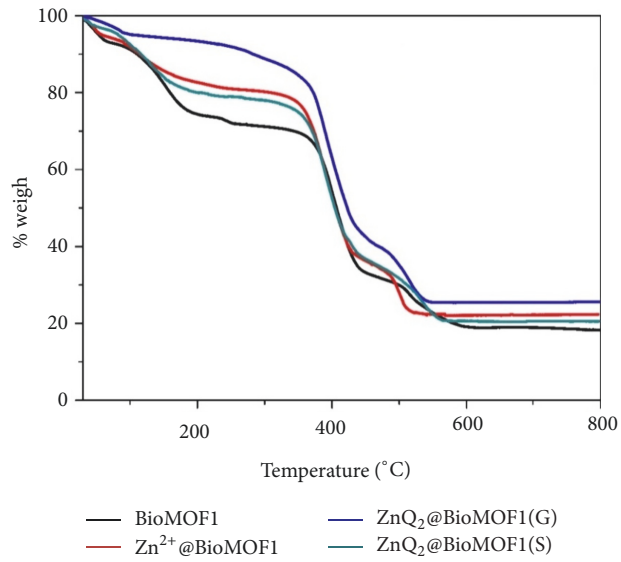

Figure 2: TGA plots of prepared BioMOF1, Zn^{2+}@BioMOF1, ZnQ_2@BioMOF1(S), and ZnQ_2@BioMOF1(G).

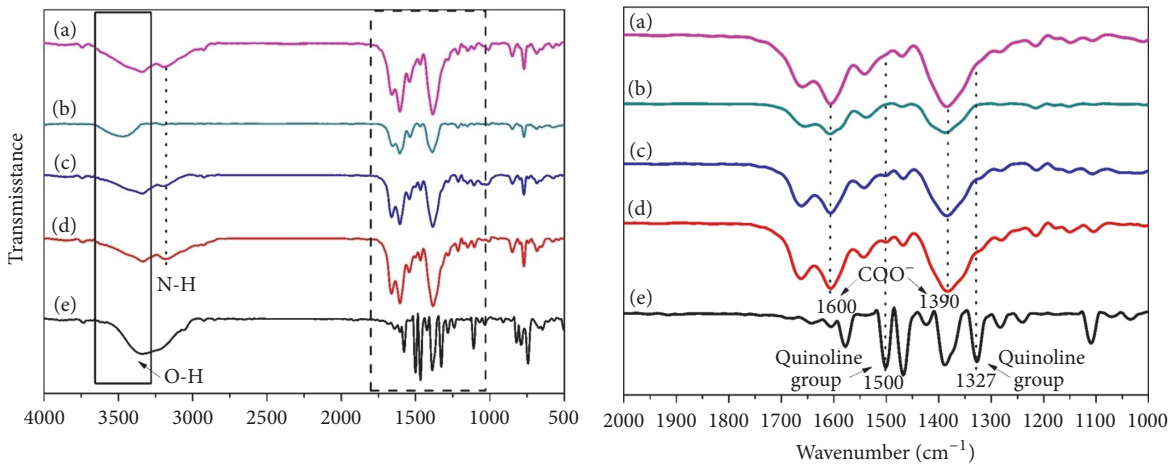

Figure 3: FTIR spectra of (a) synthesized-BioMOF1, (b) Zn^{2+}@BioMOF1, (c) ZnQ_2@BioMOF1(G), (d) ZnQ_2@BioMOF1(S), and (e) $ZnQ_2 \cdot 2H_2O$ powder.

at 250°C was assigned to the loss of DMA cations (calc. 2.72%) and the third weight loss at 380–550°C indicated the decomposition of the structure to become ZnO. It can be explained by the fact that thermal gravimetric analysis is corresponding to the elemental analysis. Therefore, from the thermal decomposition analysis, it is clear that the structure of BioMOF1 is thermally stable up to quite high temperature. Therefore, we can expect BioMOF1 to be a good host for encapsulating ZnQ_2 complexes even at high temperature.

According to elemental analysis, the percentages of elements in Zn^{2+}@BioMOF1 are found to be C, 45.28; H, 4.63; N, 12.21, which corresponds to the presence of 8 water and 4 DMF molecules. As a result, the formula can be written as Zn^{2+}@BioMOF1·4DMF·$8H_2O$ (Anal. Calc.: C, 45.90; H, 4.08; N, 11.08). This result is in agreement with the TGA analysis where the first weight loss observed from 30 to 180°C was approximately equal to 17.90%, due to the loss of 8 water and 4 DMF molecules (calc. 14.37%). The disappearance of the second-step weight loss in Zn^{2+}@BioMOF1 compared to the starting BioMOF1 implied that DMA^+ cations were replaced by Zn^{2+} ions during the cation exchange process.

The TGA curves of ZnQ_2@BioMOF1(S) and ZnQ_2@BioMOF1(G) show the similar weight loss stages compared to parent BioMOF1 and Zn^{2+}@BioMOF1, especially the last stage which corresponds to the decomposition of the BioMOF1 structures. This indicates that the structure of BioMOF1 remained intact even though ZnQ_2 guests were encapsulated in its structure.

FTIR spectra in Figure 3 showed the vibration of functional groups in $ZnQ_2 \cdot 2H_2O$, Zn^{2+}@BioMOF1, ZnQ_2@BioMOF1(S), and ZnQ_2@BioMOF1(G). The characteristic bands at around 1390, 1600 cm^{-1}, and

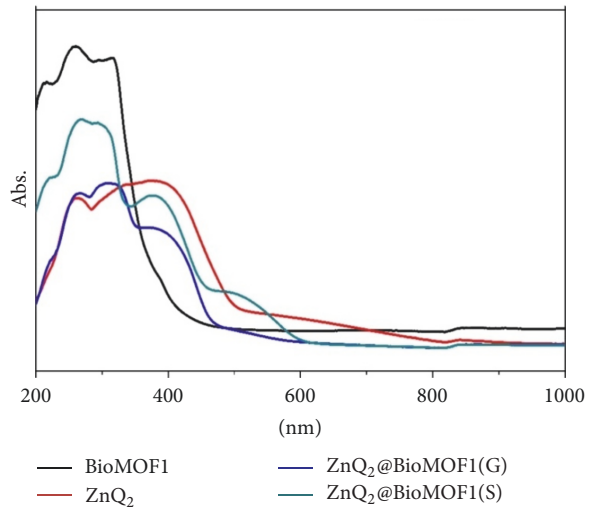

Figure 4: UV-vis absorbance spectra of solid synthesized materials.

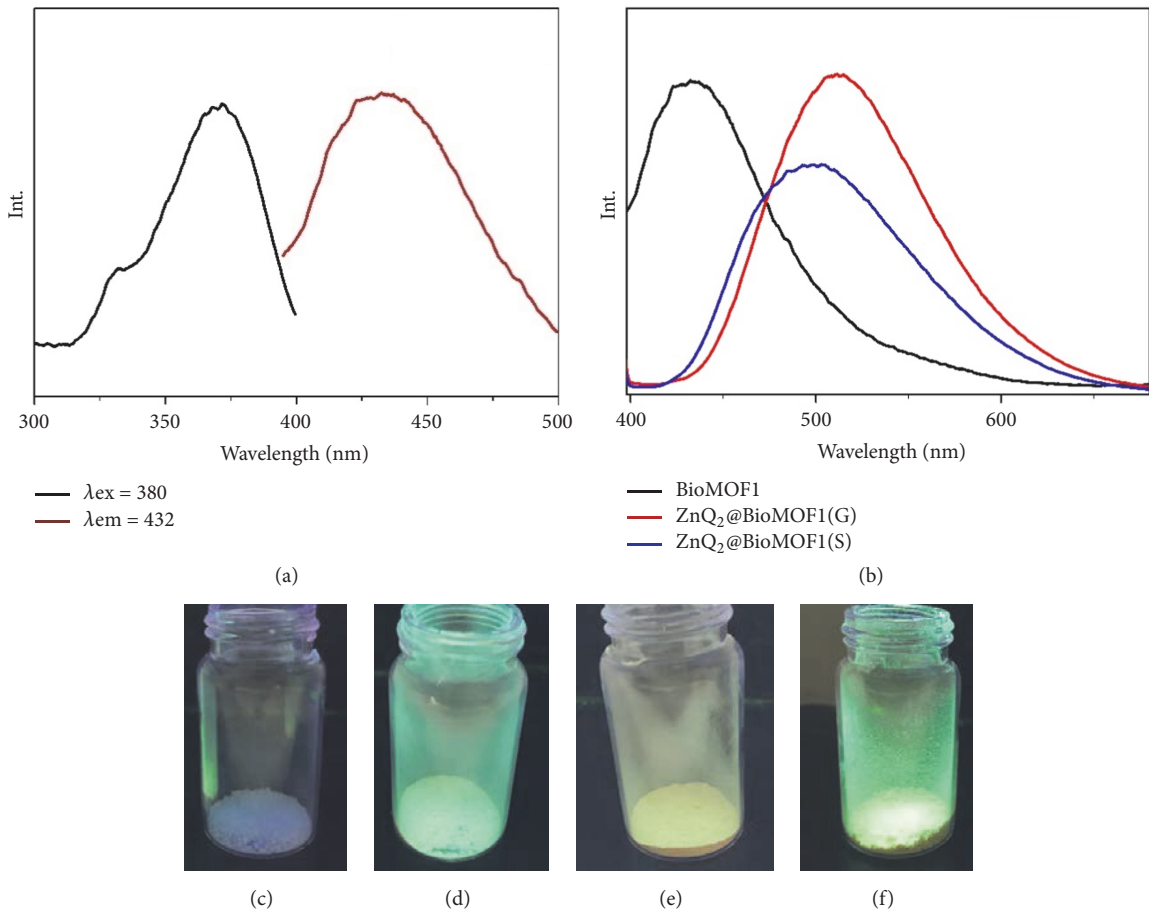

Figure 5: (a) Excitation and emission spectra of synthesized BioMOF1, (b) the fluorescence spectra of synthesized BioMOF1, ZnQ_2@BioMOF1(G), and ZnQ_2@BioMOF1(S) with the same λ_{ex} at 380 nm, (c) fluorescence photograph under UV irradiation of synthesized BioMOF1, (d) ZnQ_2@BioMOF1(S), (e) ZnQ_2@BioMOF1(G), and (f) $ZnQ_2 \cdot 2H_2O$ powder.

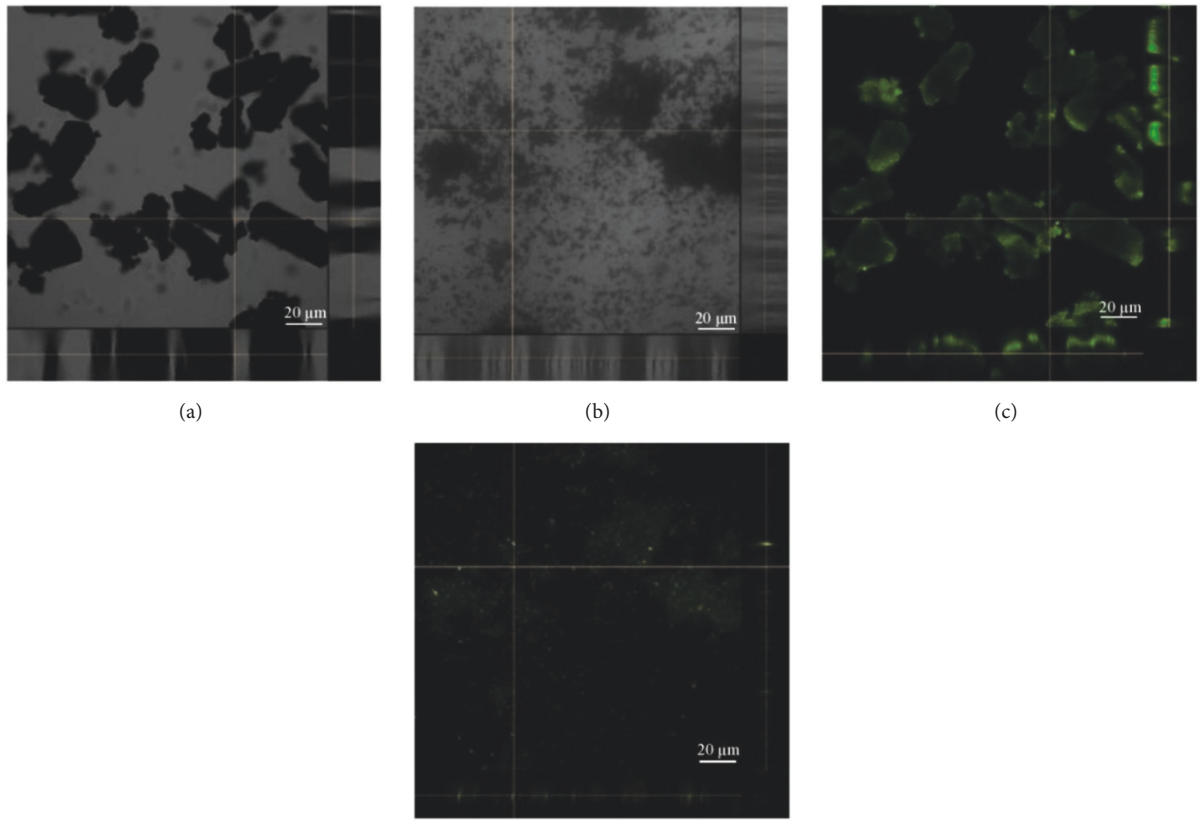

Figure 6: Photograph of (a) ZnQ_2@BioMOF1(S), (b) ZnQ_2@BioMOF1(G), and Confocal microscopy images (z-stack projection) with orthogonal cross sections (x and y directions) of (c) ZnQ_2@BioMOF1(S) and (d) ZnQ_2@BioMOF1(G).

3000–3500 cm^{-1} were observed for all the encapsulated BioMOF1 and attributed to the O-C-O stretching of carboxylate and N-H stretching of adenine ligands and water molecules, respectively. The presence of $ZnQ_2{\cdot}2H_2O$ can be confirmed by focusing on the bands existing in the region of 1000–1750 cm^{-1}. From Figure 3 (expand), the characteristic band at 1500 cm^{-1} which corresponds to the vibrations of pyridyl and phenyl groups of 8-hydroxyquinoline [40] was observed in the spectrum ZnQ_2@BioMOF1(S) and ZnQ_2@BioMOF1(G) but was absent from the spectrum of Zn^{2+}@BioMOF1. This clearly shows that $ZnQ_2{\cdot}2H_2O$ was formed in ZnQ_2@BioMOF1(S) and ZnQ_2@BioMOF1(G). In addition, the bands at 1327 cm^{-1} attributed to the quinoline group of $ZnQ_2{\cdot}2H_2O$ were found in ZnQ_2@BioMOF1(S) and ZnQ_2@BioMOF1(G) spectrum. However, this band for ZnQ_2@BioMOF1(S) and ZnQ_2@BioMOF1(G) was red-shifted, which indicates an interaction between quinoline complex and BioMOF1 frameworks.

According to Figure 4, BioMOF1 shows the absorption band in UV region, corresponding with the white color of the compound. The prepared $ZnQ_2{\cdot}2H_2O$ shows two absorption bands at 270 and 400 nm which is in agreement with literature [26]. These bands can be attributed to a π-π^* transition and metal-to-ligand charge transfer (MLCT), respectively. For ZnQ_2@BioMOF1(G) and (S), the formation of $ZnQ_2{\cdot}2H_2O$ in the pores of BioMOF1 resulted in the absorption spectrum in two absorption regions: one in the UV region similar to BioMOF1 and the other one in visible region at the same λ_{max} of $ZnQ_2{\cdot}2H_2O$ (Figure 4), indicating that encapsulation of $ZnQ_2{\cdot}2H_2O$ in the host BioMOF1 was successful. This confirmed that $ZnQ_2{\cdot}2H_2O$ complex was formed in the host BioMOF1 from both solid-solid reaction and solid-solution reaction.

The solid-state fluorescence of BioMOF1 shows blue emission band at λ_{em} 432 nm (λ_{ex} 380 nm) (Figure 5(a)) while maximum emission peak of $ZnQ_2{\cdot}2H_2O$ is found at 495 nm [26] (λ_{ex} 380 nm) with quantum yield 29.9% and life time 60.2 μs. After $ZnQ_2{\cdot}2H_2O$ were encapsulated in the pores forming ZnQ_2@BioMOF1, under the same condition (λ_{ex} 380 nm), the emission band at 432 nm disappears. Only emission band at λ_{em} 499 nm for ZnQ_2@BioMOF1(S) (quantum yield 7.23% and life time 69.3 μs) and 511 nm for ZnQ_2@BioMOF1(G) (quantum yield 6.97% and life time 57.4 μs) are present which is corresponding to $ZnQ_2{\cdot}2H_2O$ (Figure 5(b)). The fluorescence photographs of the prepared materials are shown in Figures 5(c)–5(f) with respect to fluorescence spectra of those materials. Red shift was observed in the fluorescence spectrum of ZnQ_2@BioMOF1 prepared

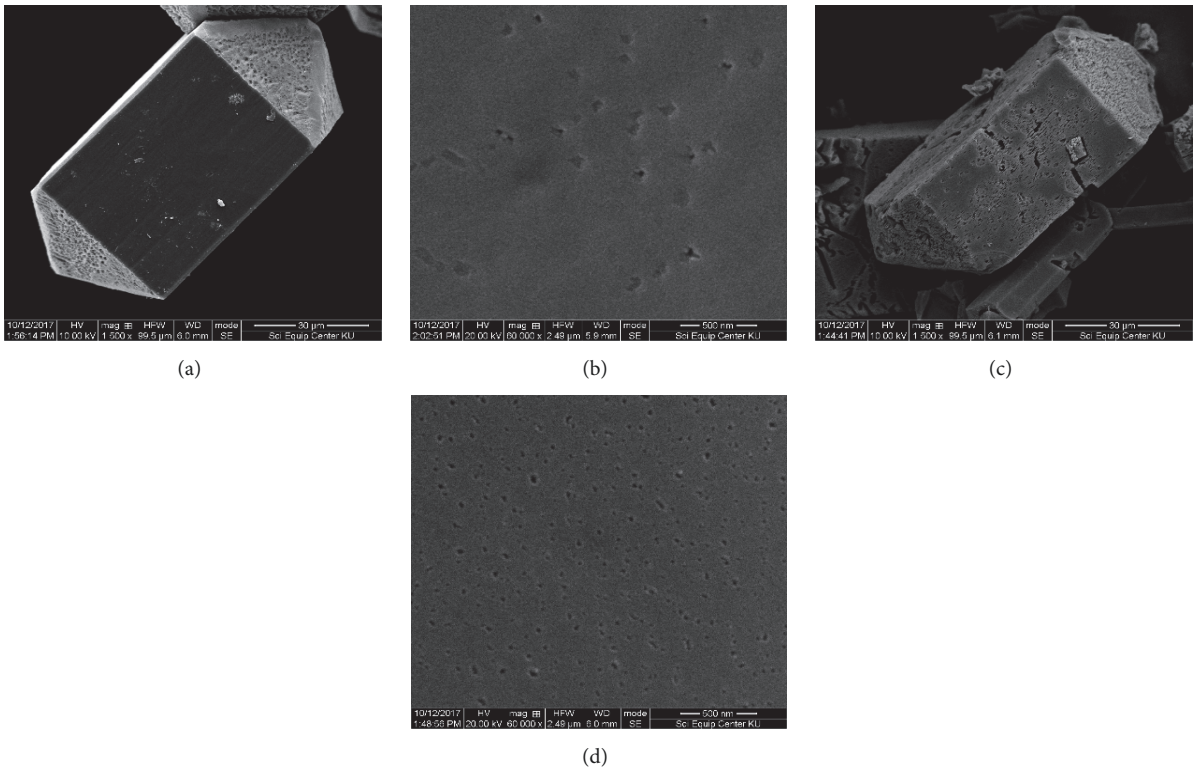

(a) (b) (c) (d)

Figure 7: Low-magnification and high-magnification SEM images of (a) and (b) synthesized BioMOF1 (c) and (d) ZnQ_2@BioMOF1(S), respectively.

by grinding compared to the one prepared by soaking. We think that it was possible from the different particle size of $ZnQ_2{\cdot}2H_2O$ [26]. The disappearance of the band at 432 nm could be assigned to photoinduced electron transfer from BioMOF1 to ZnQ_2 [41, 42] and total electron transfer was proposed. It may be close together between BioMOF1 and $ZnQ_2{\cdot}2H_2O$.

To confirm intercalation of $ZnQ_2{\cdot}2H_2O$ in the host BioMOF1, confocal fluorescence microscopy was employed. Figures 6(a) and 6(b) show photograph of ZnQ_2@BioMOF1(S) and ZnQ_2@BioMOF1(G), respectively, comparable with fluorescence images (Figures 6(b) and 6(d)) to understand the distribution of $ZnQ_2{\cdot}2H_2O$. The inset images with respect to orthogonal cross sections reveal that fluorescence species located at some depth from the surface of materials, but not on their surface, which suggests that $ZnQ_2{\cdot}2H_2O$ guests were formed within the framework of BioMOF1. Figures 7(a) and 7(b) show scanning electron microscopy (SEM) images of the microsized BioMOF1 crystal, which exhibit regular shape and smooth surface. After $ZnQ_2{\cdot}2H_2O$ was encapsulated in BioMOF1's pore by soaking (Figures 7(c) and 7(d)), the morphology and surface of ZnQ_2@BioMOF1(S) change slightly compared to the parent BioMOF1.

The Study of Dissolved Oxygen in Water Sensing. In order to study potential application of the ZnQ_2@BioMOF1(G) as a luminophore in a sensor, luminescence was measured after treating ZnQ_2@BioMOF1(S) with dissolved oxygen. The fluorescence intensity of ZnQ_2@BioMOF1 was varied as a function of amount of dissolved oxygen in water as shown in Figure 8(a). The data were also fitted to a Stern-Volmer equation:

$$\frac{I_o}{I} = 1 + K_{sv}\left[O_2\right]. \quad (1)$$

I_o and I represent the luminescent intensities in the absence and presence of O_2 gas. K_{sv} is the Stern-Volmer quenching constant which can be obtained from Stern-Volmer plot [43] (Figure 8(b)).

4. Conclusions

It can be concluded that Zn(8-hydroxyquinoline)$_2$(H_2O)$_2$ or $ZnQ_2{\cdot}2H_2O$ can be synthesized in the pores of BioMOF1 via solid-solid and solid-solution reactions by metal-cation-directed de novo assembly method without structural collapse. The photoinduced electron transfer from BioMOF1 to $ZnQ_2{\cdot}2H_2O$ occurred providing new emission band near 500 nm belonging to $ZnQ_2{\cdot}2H_2O$. A film of synthesized material on polystyrene sheet shows sensing to dissolved oxygen in water by fluorescence quenching. The fluorescence intensities can be fitted to Stern-Volmer equation but, however, Stern-Volmer quenching constant (K_{sv}) is relatively low.

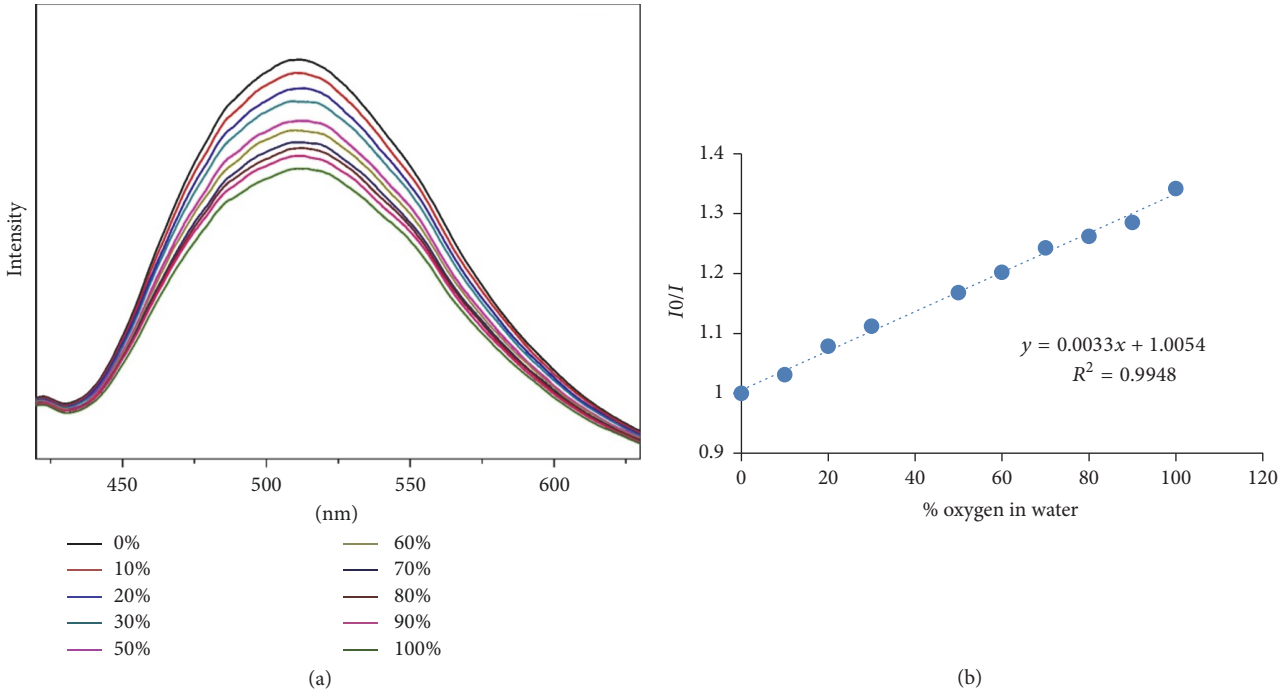

FIGURE 8: Fluorescence intensity of the ZnQ_2@BioMOF1(G) film at different percentages of DO (a) and plot of I_o/I versus % O_2 (Stern-Volmer plot) (b).

Conflicts of Interest

The authors declare that there are no conflicts of interest regarding the publication of this article.

Acknowledgments

The authors would like to thank the Department of Chemistry, Faculty of Science, Kasetsart University, the Science Achievement Scholarship of Thailand, and Kasetsart University Research and Development Institute for financially supporting this work.

References

[1] J. L. C. Rowsell and O. M. Yaghi, "Strategies for hydrogen storage in metal-organic frameworks," *Angewandte Chemie International Edition*, vol. 44, no. 30, pp. 4670–4679, 2005.

[2] C. Palomo, M. Oiarbide, and R. López, "Asymmetric organocatalysis by chiral Brønsted bases: implications and applications," *Chemical Society Reviews*, vol. 38, no. 2, pp. 632–653, 2009.

[3] D. Cunha, M. Ben Yahia, S. Hall et al., "Rationale of drug encapsulation and release from biocompatible porous metal-organic frameworks," *Chemistry of Materials*, vol. 25, no. 14, pp. 2767–2776, 2013.

[4] Z.-Z. Lu, R. Zhang, Y.-Z. Li, Z.-J. Guo, and H.-G. Zheng, "Solvatochromic behavior of a nanotubular metal-organic framework for sensing small molecules," *Journal of the American Chemical Society*, vol. 133, no. 12, pp. 4172–4174, 2011.

[5] Y. Yang, K.-Z. Wang, and D. Yan, "Ultralong Persistent Room Temperature Phosphorescence of Metal Coordination Polymers Exhibiting Reversible pH-Responsive Emission," *ACS Applied Materials & Interfaces*, vol. 8, no. 24, pp. 15489–15496, 2016.

[6] X. Yang and D. Yan, "Strongly Enhanced Long-Lived Persistent Room Temperature Phosphorescence Based on the Formation of Metal–Organic Hybrids," *Advanced Optical Materials*, vol. 4, no. 6, pp. 897–905, 2016.

[7] L. Ma, J. M. Falkowski, C. Abney, and W. Lin, "A series of isoreticular chiral metalg-organic frameworks as a tunable platform for asymmetric catalysis," *Nature Chemistry*, vol. 2, no. 10, pp. 838–846, 2010.

[8] N. Yanai, K. Kitayama, Y. Hijikata et al., "Gas detection by structural variations of fluorescent guest molecules in a flexible porous coordination polymer," *Nature Materials*, vol. 10, no. 10, pp. 787–793, 2011.

[9] G. Lu, S. Li, Z. Guo et al., "Imparting functionality to a metal-organic framework material by controlled nanoparticle encapsulation," *Nature Chemistry*, vol. 4, no. 4, pp. 310–316, 2012.

[10] S. Yang, X. Lin, A. J. Blake et al., "Cation-induced kinetic trapping and enhanced hydrogen adsorption in a modulated anionic metal-organic framework," *Nature Chemistry*, vol. 1, no. 6, pp. 487–493, 2009.

[11] C. Wang, K. E. Dekrafft, and W. Lin, "Pt nanoparticles@photoactive metal-organic frameworks: efficient hydrogen evolution via synergistic photoexcitation and electron injection," *Journal of the American Chemical Society*, vol. 134, no. 17, pp. 7211–7214, 2012.

[12] J. Yu, Y. Cui, C. Wu et al., "Second-Order nonlinear optical activity induced by ordered dipolar chromophores confined in

the pores of an anionic metal-organic framework," *Angewandte Chemie International Edition*, vol. 51, no. 42, pp. 10542–10545, 2012.

[13] J. Juan-Alcañiz, J. Gascon, and F. Kapteijn, "Metal-organic frameworks as scaffolds for the encapsulation of active species: State of the art and future perspectives," *Journal of Materials Chemistry*, vol. 22, no. 20, pp. 10102–10119, 2012.

[14] X. Yang and D. Yan, "Long-lasting phosphorescence with a tunable color in a Mn2+-doped anionic metal-organic framework," *Journal of Materials Chemistry C*, vol. 5, no. 31, pp. 7898–7903, 2017.

[15] X. Yang and D. Yan, "Long-afterglow metal-organic frameworks: Reversible guest-induced phosphorescence tunability," *Chemical Science*, vol. 7, no. 7, pp. 4519–4526, 2016.

[16] A. Corma, H. García, and F. X. Llabrés I Xamena, "Engineering metal organic frameworks for heterogeneous catalysis," *Chemical Reviews*, vol. 110, no. 8, pp. 4606–4655, 2010.

[17] J. E. Mondloch, W. Bury, D. Fairen-Jimenez et al., "Vapor-phase metalation by atomic layer deposition in a metal-organic framework," *Journal of the American Chemical Society*, vol. 135, no. 28, pp. 10294–10297, 2013.

[18] D. T. Genna, A. G. Wong-Foy, A. J. Matzger, and M. S. Sanford, "Heterogenization of homogeneous catalysts in metal-organic frameworks via cation exchange," *Journal of the American Chemical Society*, vol. 135, no. 29, pp. 10586–10589, 2013.

[19] M. H. Alkordi, Y. Liu, R. W. Larsen, J. F. Eubank, and M. Eddaoudi, "Zeolite-like metal-organic frameworks as platforms for applications: On metalloporphyrin-based catalysts," *Journal of the American Chemical Society*, vol. 130, no. 38, pp. 12639–12641, 2008.

[20] R. W. Larsen and L. Wojtas, "Photophysical studies of Ru(II)tris(2,2′-bipyridine) confined within a Zn(II)-trimesic acid polyhedral metal-organic framework," *The Journal of Physical Chemistry A*, vol. 116, no. 30, pp. 7830–7835, 2012.

[21] S. S. Tandon, L. K. Thompson, J. N. Bridson, and J. C. Dewan, "Dinuclear copper(II) and cobalt(II) complexes of the tetradentate ligand 1,2,4,5-tetrakis(benzimidazol-2-yl)benzene (BTBI): Metallacyclic and nonmetallacyclic derivatives. X-ray crystal structures of [CU2(BTBI)2Cl2][Cu2(BTBI)Cl 2(DMF)4]Cl4·12DMF and [Co2(BTBI)Br4]·4DMF," *Inorganic Chemistry*, vol. 33, no. 1, pp. 54–61, 1994.

[22] M. Yoshizawa, T. Kusukawa, M. Fujita, and K. Yamaguchi, "Ship-in-a-bottle synthesis of otherwise labile cyclic trimers of siloxanes in a self-assembled coordination cage [13]," *Journal of the American Chemical Society*, vol. 122, no. 26, pp. 6311-6312, 2000.

[23] M. Shakeri, R. J. M. Klein Gebbink, P. E. De Jongh, and K. P. De Jong, "Tailoring the window sizes to control the local concentration and activity of (salen)Co catalysts in plugged nanochannels of SBA-15 materials," *Angewandte Chemie International Edition*, vol. 52, no. 41, pp. 10854–10857, 2013.

[24] J. An, S. J. Geib, and N. L. Rosi, "Cation-triggered drug release from a porous zinc-adeninate metal-organic framework," *Journal of the American Chemical Society*, vol. 131, no. 24, pp. 8376-8377, 2009.

[25] E. Gondek, I. V. Kityk, A. Danel et al., "Electroluminescence of several pyrazoloquinoline and quinoksaline derivatives," *Materials Letters*, vol. 60, no. 27, pp. 3301–3306, 2006.

[26] R. Wang, Y. Cao, D. Jia, L. Liu, and F. Li, "New approach to synthesize 8-hydroxyquinoline-based complexes with Zn 2+ and their luminescent properties," *Optical Materials*, vol. 36, no. 2, pp. 232–237, 2013.

[27] P. Hartmann, M. J. P. Leiner, and M. E. Lippitsch, "Luminescence quenching behavior of an oxygen sensor based on a Ru(II) complex dissolved in polystyrene," *Analytical Chemistry*, vol. 67, no. 1, pp. 88–93, 1995.

[28] E. Singer, G. L. Duveneck, M. Ehrat, and H. M. Widmer, "Fiber optic sensor for oxygen determination in liquids," *Sensors and Actuators A: Physical*, vol. 42, no. 1-3, pp. 542–546, 1994.

[29] E. R. Carraway, J. N. Demas, and B. A. DeGraff, "Luminescence quenching mechanism for microheterogeneous systems," *Analytical Chemistry*, vol. 63, no. 4, pp. 332–336, 1991.

[30] J. R. Bacon and J. N. Demas, "Determination of Oxygen Concentrations by Luminescence Quenching of a Polymer-Immobilized Transition-Metal Complex," *Analytical Chemistry*, vol. 59, no. 23, pp. 2780–2785, 1987.

[31] X.-M. Li and K.-Y. Wong, "Luminescent platinum complex in solid films for optical sensing of oxygen," *Analytica Chimica Acta*, vol. 262, no. 1, pp. 27–32, 1992.

[32] W. Xu, K. A. Kneas, J. N. Demas, and B. A. DeGraff, "Oxygen sensors based on luminescence quenching of metal complexes: Osmium complexes suitable for laser diode excitation," *Analytical Chemistry*, vol. 68, no. 15, pp. 2605–2609, 1996.

[33] L. Sacksteder, J. N. Demas, and B. A. DeGraff, "Design of oxygen sensors based on quenching of luminescent metal complexes: Effect of ligand size on heterogeneity," *Analytical Chemistry*, vol. 65, no. 23, pp. 3480–3483, 1993.

[34] Z. Pang, X. Gu, A. Yekta et al., "Phosphorescent oxygen sensors utilizing sulfur-nitrogen-phosphorus polymer matrices," *Advanced Materials*, vol. 8, no. 9, pp. 768–771, 1996.

[35] Y. Amao, Y. Ishikawa, and I. Okura, "Green luminescent iridium(III) complex immobilized in fluoropolymer film as optical oxygen-sensing material," *Analytica Chimica Acta*, vol. 445, no. 2, pp. 177–182, 2001.

[36] Y. Amao, K. Asai, T. Miyashita, and I. Okura, "Novel optical oxygen pressure sensing materials: Platinum porphyrin-styrene-trifluoroethylmethacrylate copolymer film," *Chemistry Letters*, no. 10, pp. 1031-1032, 1999.

[37] H.-L. Pang, N.-Y. Kwok, L. M.-C. Chow et al., "ORMOSIL oxygen sensors on polystyrene microplate for dissolved oxygen measurement," *Sensors and Actuators B: Chemical*, vol. 123, no. 1, pp. 120–126, 2007.

[38] C. Su-ngam, S. H. Thang, A. Wongchaisuwat, and L. Meesuk, "Dissolved Oxygen Sensor Film Using Ruthenium PolypyridineComplex As Luminophore," *Journal of Metals, Materials and Minerals*, vol. 23, no. 1, pp. 61–65, 2013.

[39] B. Meier, T. Werner, I. Klimant, and O. S. Wolfbeis, "Novel oxygen sensor material based on a ruthenium bipyridyl complex encapsulated in zeolite Y: dramatic differences in the efficiency of luminescence quenching by oxygen on going from surface-adsorbed to zeolite-encapsulated fluorophores," *Sensors and Actuators B: Chemical*, vol. 29, no. 1-3, pp. 240–245, 1995.

[40] N. Chuekuna, A. Wongchaisuwat, and L. Meesuk, "Zinc-8-hydroxyquinoline intercalated in calcium bentonite: A promising DO sensor," *Journal of Physics and Chemistry of Solids*, vol. 71, no. 4, pp. 423–426, 2010.

[41] D. Yan, Y. Tang, H. Lin, and D. Wang, "Tunable two-color luminescence and host-guest energy transfer of fluorescent chromophores encapsulated in metal-organic frameworks," *Scientific Reports*, vol. 4, article no. 4337, 2014.

[42] Y. Tang, W. He, Y. Lu, J. Fielden, X. Xiang, and D. Yan, "Assembly of ruthenium-based complex into metal-organic framework

with tunable area-selected luminescence and enhanced photon-to-electron conversion efficiency," *The Journal of Physical Chemistry C*, vol. 118, no. 44, pp. 25365–25373, 2014.

[43] M. M. F. Choi and D. Xiao, "Single standard calibration for an optical oxygen sensor based on luminescence quenching of a ruthenium complex," *Analytica Chimica Acta*, vol. 403, no. 1-2, pp. 57–65, 2000.